I&EC research
Industrial & Engineering Chemistry Research
pubs.acs.org/IECR
Article

Efficient Growth of Carbon Nanotube Carpets Enabled by In Situ Generation of Water

Brian M. Everhart,[‖] Haider Almkhelfe,[‖] Xu Li, Michael Wales, Pavel Nikolaev, Rahul Rao, Benji Maruyama, and Placidus B. Amama*

Cite This: *Ind. Eng. Chem. Res.* 2020, 59, 9095−9104

ABSTRACT: Catalytic chemical vapor deposition (CVD) utilizing the gaseous product mixture of Fischer−Tropsch synthesis (FTS-GP) offers the potential for scale-up and controlled growth of carbon nanotube (CNT) carpets. In comparison to conventional feedstocks, FTS-GP exhibits the ability to support an exceptionally long catalyst lifetime with Fe catalysts. The role of the feedstock in growth enhancement is still poorly understood. In this study, a combination of experimental and thermodynamic analyses reveal on-site generation of water to be the secret for observed growth enhancement in FTS-GP CVD. The concentration of water generated in situ decreases with increasing reactor temperature. Further investigations using an Autonomous Research System (ARES)—an automated, high-throughput, laser-induced CVD system with in situ Raman spectral feedback—reveal FTS-GP not only exhibits exceptionally long catalyst lifetimes compared to a standard feedstock (C_2H_4), but also shows a high tolerance for relatively high levels of water.

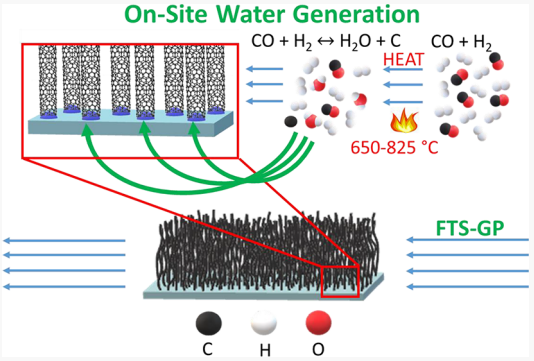

1. INTRODUCTION

The emergence of carbon nanotube (CNT) carpets, consisting of self-aligned nanotubes produced via catalytic chemical vapor deposition (CVD) from densely packed catalyst nanoparticles on a substrate, has inspired application opportunities in many important areas.[1−9] Scale-up of the process is often plagued by complicated optimization procedures due to the high sensitivity of the growth process to variations in feedstock composition, flow characteristics, and reactor geometry.[10−12] Single-walled CNT (SWCNT) carpet growth experienced a major boost with the discovery of "supergrowth", a process that leads to dramatic enhancement in catalytic activity upon the addition of a small amount of water.[8,13,14] Other oxygen-containing feedstocks or additives such as ethanol,[15,16] acetone,[17] CO,[17−19] and CO_2[19−22] have also shown the ability to promote SWCNT carpet growth. However, as shown by a number of studies, determining the optimum amount of oxidant required for efficient growth remains a challenge. Xie et al.[23] revealed that growth rate and catalyst lifetime during "supergrowth" have high sensitivity to water concentration. At optimum water concentration (∼200 ppm), high lifetime (>1065 s) and growth rate (∼0.13 g_{CNTs} g^{-1}_{cat} s^{-1}) can be achieved, whereas operating below or above this level of water results in a decrease in CNT yield. Szabó et al.[24] observed the presence of water vapor in the feed yielded CNT carpets of higher quality, but at the expense of carpet height; the effects were attributed to the oxidizing property of water. In light of increasing global demand for CNTs,[7] there is a need to develop approaches that maximize yield, minimize production cost, and have process conditions relatively easier to optimize.

Catalytic CVD, utilizing the gaseous product mixture of Fischer−Tropsch synthesis (FTS), offers the possibility of scaling up synthesis of CNTs due to its high growth efficiency.[25,26] FTS is a gas-to-liquid polymerization process that transforms syngas (mixture of CO and H_2) into liquid hydrocarbons. Based on the Anderson−Schulz−Flory model that predicts the distribution of products from FTS, even at optimum probability of chain growth, a substantial yield of low-molecular-weight gaseous products is unavoidable.[27] The gaseous product mixture from FTS (referred to as FTS-GP) usually consists of a variety of C1−C4 hydrocarbons and unreacted CO and H_2. As demonstrated in prior studies, FTS-GP is a promising feedstock for efficient CVD growth of SWCNT[26] and multiwalled CNT (MWCNT) carpets under a broad range of conditions.[25] A comparison of growth profiles (carpet height as a function of growth time) of SWCNT carpets from FTS-GP CVD, using Fe catalysts and other conventional CVD processes with different feedstocks, reveals a relatively high growth rate (∼50 μm/min) and a catalyst

Received: February 11, 2020
Revised: April 13, 2020
Accepted: April 13, 2020
Published: April 13, 2020

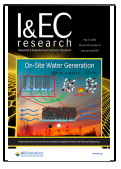

https://dx.doi.org/10.1021/acs.iecr.0c00711
Ind. Eng. Chem. Res. 2020, 59, 9095−9104

lifetime (>90 min) superior to other CVD approaches.[26,28] Use of FTS-GP as a feedstock has multiple benefits. First, it does not require stringent optimization of process conditions as it appears to have a broad window for growth of SWCNT carpets. Second, it has an uncommon feature of not only supplying a high flux of carbon species to the catalyst particles, but also protecting them from early loss of activity. Third, in light of increasing global demand for CNTs, use of FTS-GP as a feedstock in industrial-scale production is expected to minimize gaseous waste in FTS plants. Further improvement, control, and scale-up of FTS-GP CVD will require a good understanding of the role of FTS-GP in CNT growth enhancement.

Here, we hypothesize water formed by a reaction between H_2 and the low-volume fraction of CO in FTS-GP is responsible for enhanced growth efficiency characteristic of FTS-GP CVD. The water, formed in the vicinity of the catalyst during the process as illustrated in Figure 1, is expected to play

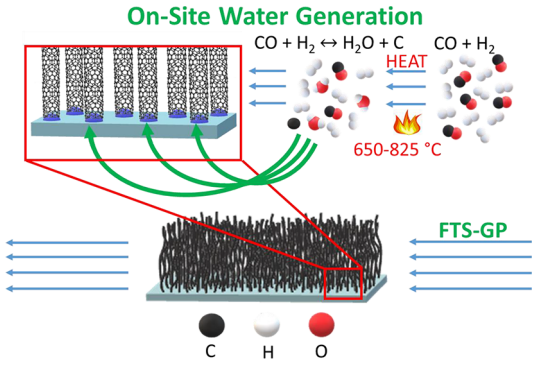

Figure 1. Schematic illustration of on-site generation of water during CNT carpet growth via FTS-GP CVD.

a similar role as reported for "supergrowth": oxidizing carbon contaminants deposited on the catalyst surface[8,29] and inhibiting mass loss (Ostwald ripening and subsurface diffusion) during SWCNT growth, thus extending catalyst lifetime.[30−35] We study the role of FTS-GP in CNT growth using a combination of experimental and theoretical methodologies. Thermodynamic analysis investigates feasibility of the reaction between water and CO at different growth temperatures and estimates the amount of water generated under our CVD conditions.The first experimental approach involves direct analysis of gas-phase products from thermal decomposition of FTS-GP in a batch reactor (without the catalyst) at different reaction temperatures (650, 700, 750, and 800 °C). Second, due to the breadth of parameters that affect CVD growth of SWCNTs, rapid experimentation is necessary for effective optimization of growth conditions and understanding of the role of feedstock in growth. Here, we employ an Autonomous Research System (ARES)[36,37]—an automated, high-throughput, laser-induced CVD system with in situ Raman spectral feedback—to measure SWCNT growth kinetics and compare the differences in growth with FTS-GP and a conventional feedstock (C_2H_4) in the presence and absence of water. Illumination of the complex interdependence of growth parameters and the role of FTS-GP in growth enhancement is expected to provide a rational framework for potential optimization and scale-up of CNT growth via FTS-GP CVD.

2. EXPERIMENTAL SECTION

2.1. SWCNT Growth by FTS-GP CVD. A thin Fe film supported on an amorphous alumina film (Al_xO_y/Fe) was used as the catalyst for SWCNT carpet growth. The films were deposited by an ion beam sputter deposition and etching system (IBS/e, South Bay Technology) on Si(100) substrates with a native oxide layer (P type and B-doped) at 10^{-4} Torr chamber pressure without exposing the films to air between depositions. Nominal thicknesses of Fe and Al_xO_y films were 1.3 and 30 nm, respectively. Thicknesses of the films deposited were measured by a quartz crystal thickness monitor and corroborated by height profile measurements using an atomic force microscope. The feedstock used was FTS-GP (supplied by Matheson Inc.) with the composition CO (5%), C_2H_6 (8%), C_2H_4 (6%), CH_4 (30%), N_2 (4%), C_3H_8 (5%), H_2 (40%), and C_3H_6 (2%),[38−40] which is similar to the typical composition of a gaseous product mixture for FTS and hydrocracking processes in the presence of Fe catalysts.[41]

SWCNT growth was carried out at atmospheric pressure with the use of the EasyTube 101 CVD system (CVD Equipment Corp.) equipped with several features for improved process control including LabView-based process control software, a static mixer for optimum gas mixing, and a control system for precise temperature control. A typical growth experiment involved heating the Al_xO_y/Fe catalyst to the desired temperature (650, 700, 750, or 800 °C) at a rate of 45 °C/min in flowing Ar. Once at the growth temperature, the catalyst was reduced for 10 min by the introduction of hydrogen; the respective flow rates were 250 standard cubic centimeters per minute (sccm) H_2 and 250 sccm Ar. Thereafter, SWCNT growth was initiated at the respective temperatures by the introduction of FTS-GP in combination with Ar as the diluent (100 sccm FTS-GP and 1000 sccm Ar) for different durations. At the end of each growth experiment, samples were rapidly cooled in H_2 followed by slow cooling to room temperature in 700 sccm Ar.

2.2. Characterization. The morphologies and quality of the grown SWCNT carpets were characterized by field emission scanning electron microscopy (SEM; FEI-Versa 3D DualBeam) and Raman spectroscopy. Raman spectroscopic characterization was carried out in a Renishaw in Via Raman microscope using a laser excitation wavelength of 633 nm. Heights of tall carpets (>0.5 μm) were measured using an optical microscope.

Products formed during FTS-GP CVD in a batch reactor were analyzed by a Hewlett-Packard 6890 series gas chromatograph (GC) with a thermal conductivity detector (TCD). The injector port was held constant at 170 °C, and was operated in slip mode with a 150:1 split ratio using a split liner with deactivated wool (Agilent 5183-4711). Samples were separated using a nonpolar column connected in series with a polar column HP-5 (Agilent 19091J-413) and DB-Wax (Agilent 122-7032), respectively. Columns were connected using a press-fit connector (Agilent 5190-6979) and operated in constant flow (1.2 mL/min) with He as a carrier gas. The GC temperature was initially at 50 °C and held at this temperature for 1 min, followed by a ramp of 20 °C/min to a final temperature of 200 °C; the total run time was 8.5 min. The detector was maintained at 150 °C with He as the reference gas.

2.3. SWCNT Growth Investigations in ARES. Growth experiments in ARES were performed at a pressure of 20 Torr

https://dx.doi.org/10.1021/acs.iecr.0c00711
Ind. Eng. Chem. Res. 2020, 59, 9095−9104

and a temperature of 825 °C. ARES growth substrates contain silicon micropillars fabricated by reactive ion etching. Each substrate contains a 12 × 12 array of patches, each consisting of a 5 × 5 array of 10-μm-diameter, 10-μm-high silicon pillars (on an SiO_2 underlayer) coated with a 10-nm-thick Al_xO_y support layer and a 1-nm-thick Fe catalyst film. The support and catalyst layers were also deposited by IBS/e following steps described earlier for catalysts used in conventional CVD. A high power (6 W, Verdi) laser (532 nm) serves as both the heat and Raman excitation sources. The Si micropillars were heated to growth temperatures by regulating the laser power, and temperatures were estimated from the red shift of the Raman peak frequency of the Si micropillar. During each growth experiment, Raman spectra were collected every 5 s and experiments were allowed to proceed until SWCNT growth appeared to cease, as determined by a plateauing of the intensity of the SWCNT Raman peak (G band).

Growth profiles were obtained by measuring the G-band areas, and each profile was fit to a radioactive decay model (explained in detail in section 3) to extract initial growth rates and catalyst lifetimes. Water concentration in the system was measured by a dew-point sensor (Shaw) placed at the inlet of the growth chamber. For each experiment, the water concentration represents the amount of water added to the system relative to the baseline concentration (2.0−4.5 ppm). Gas lines were purged until baseline water concentrations fell below 4.5 ppm before experiments began. Experiments were conducted with the different feedstocks (FTS-GP and C_2H_4) without a diluent gas.

3. RESULTS AND DISCUSSION

3.1. Catalytic Performance at Different Temperatures. Figure 2 summarizes CNT carpet growth data at 650, 700, 750, and 800 °C using FTS-GP as a feedstock. Dense nanotube carpets with uniform coverage across the substrates were grown at these temperatures as shown by the SEM images. The selectivity of SWCNT is highest at 750 °C for Fe catalysts with the lowest amounts of MWCNTs.[26]

After performing growth for 90 min at the different temperatures, SWCNT carpets of strikingly different heights were obtained. From the SEM data in Figure 2a−d, measured heights of the resulting SWCNT carpets after 90 min of growth at 650, 700, 750, and 800 °C were 250, 625, 4000, and 970 μm, respectively. Analysis of the growth profiles in Figure 2e provides a better understanding of the catalytic performance (activity and lifetime) at the different temperatures. The evolution of nanotube carpet height with time is generally characterized by a high growth rate at the onset that subsequently decreases gradually until complete growth termination occurs.[13,26,42−44] Futaba et al.[13] showed the growth profile of SWCNT carpets during "supergrowth" to be analogous to the radioactive decay process whereby catalysts lose their activity over time. Therefore, SWCNT carpet growth can be modeled by the radioactive decay model (eq 1):

$$H(t) = \beta\tau_0(1 - e^{-t/\tau_0}) \quad (1)$$

where H is the carpet height at various times, t, while fitting parameters β and τ_0 represent the initial growth rate and characteristic catalyst lifetime, respectively. Based on the goodness of fit ($R^2 \geq 0.971$), the curve fitting of the model to the growth data at different temperatures, shown in Figure 2e, is quite good.

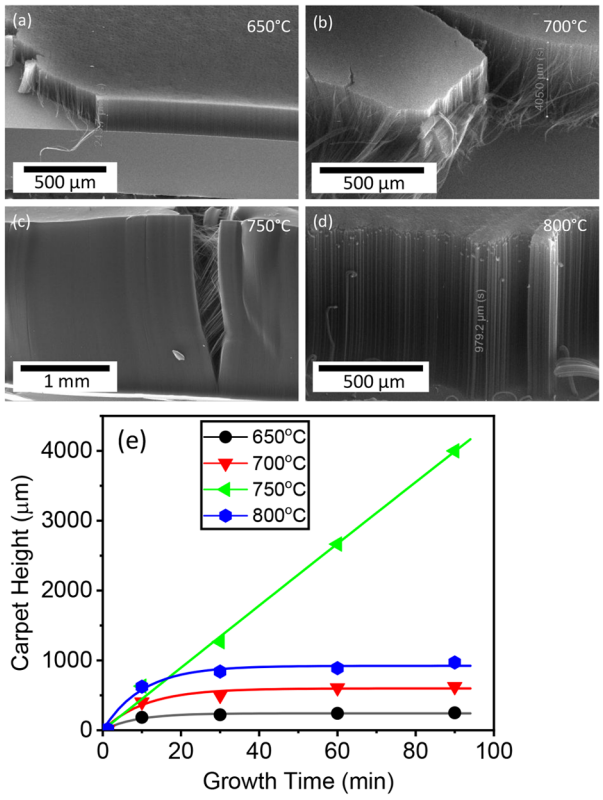

Figure 2. SEM images of SWCNT carpets grown on Al_2O_3/Fe substrates at different temperatures after 90 min: (a) 650, (b) 700, (c) 750, and (d) 800 °C. (e) Plots of SWCNT carpet height as a function of growth time for different growth temperatures; solid lines represent curve fitting of the radioactive decay model (eq 1) to the experimental data shown in symbols.

Fitting parameters for the different temperatures and goodness of fit are summarized in Table 1. The activity and lifetime of catalysts in FTS-GP CVD are highly sensitive to the growth temperature. Even though signs of deactivation are not apparent after 90 min for growth at 750 °C, fitting parameters are also extracted for comparison; we note, in all likelihood, unlike the value of β, the value of τ_0 has a large uncertainty due to the absence of any sign of deactivation within 90 min. As a result, even though the fitting parameters for growth at 750 °C are shown, the experimental value of τ_0 is considered as the lower bound and is used for comparisons.

Table 1. Summary of Fitting Parameters (β and τ) and Goodness of Fit, Modeled by the Radioactive Decay Model (eq 1), for Different Growth Temperatures

growth temp (°C)	growth rate (β) (μm/min)	lifetime (τ_0) (min)	R^2
650	28.9	8.4	0.979
700	55.3	10.8	0.971
750	44.9	3975.0	0.997
800	91.4	10.1	0.985

A long catalyst lifetime, with not many parallels in the literature for conventional CVD with a monometallic catalyst, is observed at 750 °C as the catalyst stays active after 90 min of growth and experiences no sign of deactivation during growth.

https://dx.doi.org/10.1021/acs.iecr.0c00711
Ind. Eng. Chem. Res. 2020, 59, 9095−9104

On the other hand, growth at a lower (700 °C) or higher temperature (800 °C) resulted in a significant drop in catalyst lifetime. Growth at low temperature (650 °C) exhibits a low growth rate accompanied by a short catalyst lifetime. At higher temperatures (>650 °C), the growth rate generally increases while the lifetime remains roughly the same for all temperatures (~10 min), except at our optimum growth temperature (750 °C). Maximum fitted carpet heights predicted from the product of the two fitting parameters in the model (β and τ_0) are 243 μm at 650 °C, 599 μm at 700 °C, 179 mm at 750 °C, and 923 μm at 800 °C. We assume that the catalyst lifetime for growth at 750 °C is longer than 90 min because growth termination during FTS-GP CVD does not appear to be instantaneous.[25,26,44] Therefore, except for growth at 750 °C, maximum fitted carpet heights are within the same range as experimental carpet heights for the growth temperatures. In other words, maximum carpet heights are most likely attained for growth at 650, 700, and 800 °C, and are significantly lower than the theoretical carpet height at 750 °C, as well as the experimental height of ~4 mm after 90 min of growth.

The Raman spectra of SWCNT carpets grown at different temperatures are shown in Figure 3. In addition to the

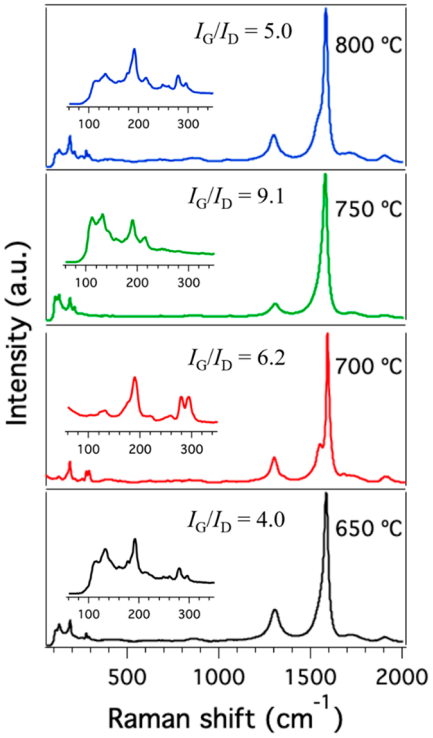

Figure 3. Representative Raman spectra of SWCNT carpet samples (excitation at 633 nm) with their respective I_G/I_D ratios.

omnipresent D and G bands associated with SWCNTs, radial breathing mode peaks (RBMs) in the low-frequency region, characteristic of SWCNTs, are observed in all spectra. The G-band peak corresponds to in-plane C−C vibrations, while the D band is attributed to carbon impurities and defects present in the CNTs. The presence of RBMs (Figure 3) suggests the presence of SWCNTs in the carpet samples. From the intensity ratios of the G band (I_G) and D band (I_D) in Figure 3 and TEM analysis,[26] carpets grown at 750 °C, a temperature that supports the longest catalyst lifetime, have the highest quality as evidenced by the highest I_G/I_D of 9.1 and SWCNT selectivity.

To facilitate comparisons between the SWCNT growth efficiency of FTS-GP CVD and conventional growth processes, we use representative studies involving monometallic catalysts in the literature to generate a catalyst lifetime versus growth rate map (Figure 4).[10,13,22,29,30,43,45−52] As reported by Chen et

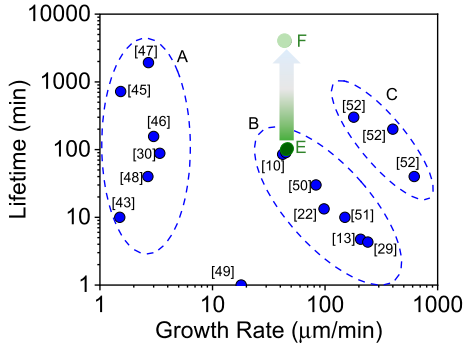

Figure 4. Growth rate−catalyst lifetime map of SWCNT carpets using supported monometallic catalyst showing a comparison of representative studies (blue) including our results from FTS-GP CVD using an Fe catalyst (green). *E* and *F* show the experimental and fitted lifetimes for FTS-GP CVD growth at 750 °C, respectively; *E* and *F* and are assumed to be the limits of τ_0. The number indicates the reference for each datum.

al.,[53] achieving a high growth rate and long catalyst lifetime simultaneously during SWCNT carpet growth is difficult due to the inverse relationship between the two, a behavior that may intrinsically be connected to growth mechanisms. The growth map showing fitting parameters (β and τ_0), adapted from Yasuda et al.,[52] exhibits three main regions. The first, on the left side of the map (A), is characterized by long catalyst lifetimes but low growth rates. Conversely, the second region, on the right side of the map (B), is characterized by rapid growth rates but short catalyst lifetimes. Increased growth rates of catalysts in region B are attributed to the presence of an oxidizer that serves as a growth enhancer to improve resistance to catalyst deactivation during rapid growth, and control of the gas-flow direction in some of the studies. Data in region C represent an improvement of "supergrowth" studies in region B, whereby control of the dwell time of the carbon feedstock and the carbon flux to the catalyst are used to overcome the inverse relationship between lifetime and growth rate.[52] The corresponding performance of FTS-GP CVD from fitting with eq 1 shows an estimated lifetime (*F*) that is quite long, albeit with high uncertainty. For meaningful comparison, the experimental value (*E*) is also included in the map. The lifetimes are shown with an arrow pointing from *E* to *F*—points we have assumed to be the lower and upper bounds, respectively, because growth cessation does not appear to be instantaneous. FTS-GP CVD, without any modification in the gas-flow direction or control of dwell time, exhibits a catalyst performance (based on experimental data) superior to studies in region A and lower bound that is at par with region B. In the following sections, a combined thermodynamic and experimental study is carried out to probe the role of FTS-GP in observed growth enhancement.

3.2. Thermodynamic Prediction of In Situ Generation of Water. The high growth efficiency of FTS-GP CVD is attributed to the simultaneous high flux of carbon species to

https://dx.doi.org/10.1021/acs.iecr.0c00711
Ind. Eng. Chem. Res. 2020, 59, 9095−9104

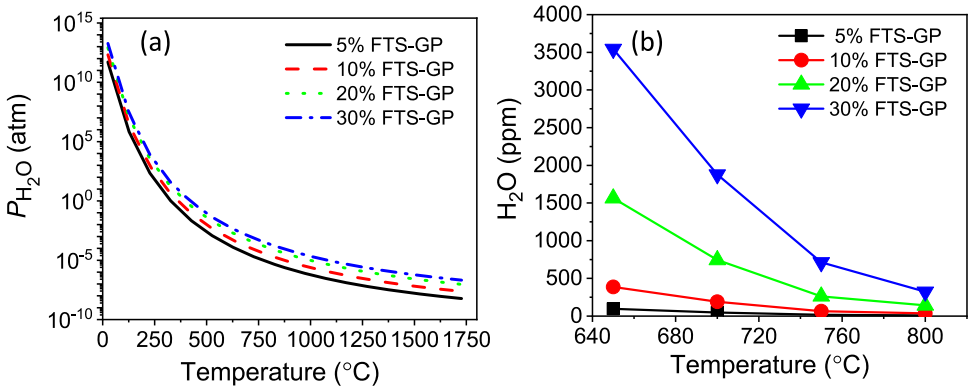

Figure 5. Thermodynamic prediction of the concentration of water generated during FTS-GP CVD. (a) Profiles of partial pressures of water as functions of growth temperatures for different feed compositions of FTS-GP (5, 10, 20, and 30%) with Ar as balance over a broad temperature range (0−1750 °C). Along these lines, ΔG of reaction R1 is zero; i.e., it is in equilibrium. (b) Profiles of water concentrations (ppm) as functions of temperatures with data points corresponding to growth temperatures used during FTS-GP CVD [adapted from (a)].

the catalyst and oxidative removal of excess amorphous carbon from the catalyst surface by water generated in situ.[25] The generation of water is hypothesized to occur via a reaction between CO and hydrogen:

$$CO_{(g)} + H_{2(g)} \leftrightarrow H_2O_{(g)} + C_{(s)} \quad \text{(R1)}$$

The reaction involving CO has two distinct pathways depending on its partial pressure: at higher partial pressure of CO, the Boudouard reaction is favored, whereas a reaction between hydrogen and CO (reaction R1) is favored at a lower partial pressure of CO and temperatures higher than 400 °C ($\Delta G = -90$ kJ/mol).[18,54,55] The conditions for reaction R1 are quite similar to our SWCNT growth conditions in FTS-GP CVD, evidenced by the low-volume fraction of CO in the feedstock (5 vol % in FTS-GP) and growth temperatures greater than 400 °C. Our objectives in this section are to (1) carry out a thermodynamic analysis to determine the feasibility of reaction R1 and (2) estimate the amount of water generated under FTS-GP CVD conditions. Using data for free energy of formation (ΔG) with respect to temperature presented on FactWeb,[56] $\Delta G^\circ(T)$ values for CO, H_2, H_2O, and C at standard conditions (1 atm of pressure) were obtained.

ΔG° for the reaction (ΔG°_{rxn}) is calculated using eq 2:

$$\Delta G^\circ_{rxn} = \sum n\Delta G^\circ_f(\text{products}) - \sum n\Delta G^\circ_f(\text{reactants}) \quad (2)$$

The free energy of formation ΔG° as a function of temperature for CO, H_2, H_2O, and C is given as

$$\Delta G^\circ_{rxn} = \Delta G^\circ(H_2O) + \Delta G^\circ(C) - \Delta G^\circ(H_2) - \Delta G^\circ(CO) \quad (3)$$

To calculate the ΔG under nonstandard conditions, ΔG is expressed as

$$\Delta G = \Delta G^\circ + RT \ln Q \quad (4)$$

where Q is the reaction quotient and given as

$$Q = \frac{P_{H_2O}}{P_{H_2}P_{CO}} \quad (5)$$

Since the partial pressure of water is unknown, ΔG cannot be determined. However, at thermodynamic equilibrium, $\Delta G = 0$, the equilibrium partial pressure of water (P_{H_2O}) can be calculated as follows:

$$P_{H_2O} = P_{CO}P_{H_2}\exp\left(-\frac{\Delta G^\circ}{RT}\right) \quad (6)$$

Partial pressures of CO and H_2 were determined for different feed compositions (0.05, 0.1, and 0.3 fractions) assuming 5% CO and 40% H_2. An important assumption in this analysis is that reaction R1 proceeds on a small-enough scale that it does not significantly alter the partial pressures of H_2 and CO. Using the calculated ΔG° as a function of temperature, equilibrium water pressures (P_{H_2O}) for the respective temperatures were obtained from eq 6.

Profiles of the predicted equilibrium partial pressure as a function of temperature for different feed compositions (5, 10, 20, and 30% FTS-GP) are shown in Figure 5a. Water concentrations in parts per million (ppm) in the temperatures that correspond to the SWCNT growth data are adapted from Figure 5a and shown in Figure 5b. Along the plot lines in Figure 5b, ΔG of reaction R1 is zero (i.e., in equilibrium). Therefore, if the partial pressure of water for a particular temperature is below these lines, ΔG of reaction R1 is negative, and the forward reaction is favored. Conversely, if the partial pressure of water for a particular temperature is above these lines, ΔG of reaction R1 is positive, and the reverse reaction will be favored. In other words, these plot lines are essentially the maximum partial pressure of water that can be generated at a particular temperature via reaction R1. An inverse relationship between the concentration of water generated and temperature is observed for all FTS-GP compositions studied (Figure 5 and Table S1). We therefore conclude the equilibrium partial pressure of water is strongly dependent on temperature.

We note that if reaction R1 is incomplete, the actual water concentration produced may be less, and if it goes to completion, the predicted concentration of water generated is expected to be far lower than that of CO, which is 2500, 5000, and 15 000 ppm for 5, 10, and 30% FTS-GP, respectively. Water concentrations obtained from this thermodynamic calculation are upper limits for the various growth conditions. Predicted concentrations of water generated for the FTS-GP fraction used in this study (10% FTS-GP) at 650, 700, 750, and 800 °C are 386.5, 190.7, 64.6, and

https://dx.doi.org/10.1021/acs.iecr.0c00711
Ind. Eng. Chem. Res. 2020, 59, 9095−9104

34.6 ppm, respectively. Interestingly, the concentration of water generated for reactions with a low FTS-GP fraction is rather low (~3 ppm for 0.05 fraction, 850 °C temperature), while for high FTS-GP fraction it is fairly large (~3200 ppm for 0.3 fraction, 650 °C temperature). Small amounts of water are generally beneficial to growth, while excess amounts tend to be detrimental.[23] Assuming reaction R1 goes to completion, it is important to understand whether relatively high levels of water generated during FTS-GP CVD are beneficial for SWCNT carpet growth.

3.3. Experimental Verification of Water Generation. The concentration of water generated during the gas-phase reaction of FTS-GP in a batch reactor was investigated as a function of temperature in the absence of a catalyst (Figure 6),

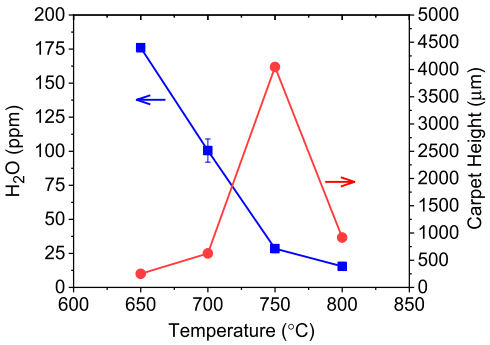

Figure 6. Concentration of water produced via gas-phase reaction of FTS-GP in a batch reactor as a function of temperature. Plot of carpet height after 90 min of growth versus temperature is included for comparison.

and the data are presented along with the experimental carpet height attained after 90 min for the respective temperatures. The absence of the catalyst invalidates the argument that water is generated via the reduction of Fe_2O_3.

In agreement with the thermodynamic prediction, the concentration of water generated during decomposition of FTS-GP decreases with increasing temperature. Even though the concentration of water measured experimentally is lower than the concentration predicted by a factor of ~2, the trends are consistent with decreasing slope at higher temperatures. In light of the dependence of SWCNT growth steps (such as feedstock decomposition, catalyst stability, and CNT nucleation) on temperature, the generation of different concentrations of water at different temperatures convolutes the role of water. It is possible using growth conditions optimized at 750 °C for growth at other temperatures may be partly responsible for the stark difference in growth kinetics.

3.4. Using ARES to Probe the Effect of Water Concentration. To further understand the role of water in FTS-GP CVD, growth experiments were performed in ARES[36,37] with C_2H_4 or FTS-GP as a feedstock at a constant temperature (825 °C) in the presence of different concentrations of water. The presence of water, depending on the amount, can lead to growth enhancement, catalyst oxidation (high water level), or catalyst deactivation via coking or mass loss (low water level). An additional amount of water (up to 24 ppm) was added in our study to probe the water tolerance of SWCNT growth with the feedstocks. As described in detail in the Experimental Section, growth experiments in ARES are performed in a cold-wall CVD chamber where a high power laser is the heat source and Raman excitation source, and Raman spectra are collected continuously during growth in order to monitor growth kinetics. Even though ARES utilizes a cold-wall reactor for growth, the effect of temperature on SWCNT growth followed the same trend as observed in conventional hot-wall CVD (Figure S1). Here we used the maximum G-band intensity at the end of the growth experiment as a proxy for yield. SWCNT yield and quality (I_G/I_D) increased with temperature, reached a maximum at 825 °C (higher than the optimum temperature of 750 °C for FTS-GP CVD), and then decreased continuously. The difference in the optimum temperature between conventional CVD and ARES could be attributed to limited or the possible absence of gas-phase decomposition of the feedstock in the latter.

SWCNT growth curves obtained from ARES at 825 °C using different feedstocks in the presence of 0, 11.8, and 23.6 ppm water were fitted with the radioactive decay model (eq 1). Representative curves of SWCNT yield (G-band integrated area) versus growth time with the fits are shown in Figure 7, while extracted initial growth rates and lifetimes are shown in Figure 8. Growth rates of SWCNTs (Figure 8a) were significantly higher with C_2H_4 as the feedstock compared to FTS-GP. For both feedstocks, the growth rate decreased with increasing concentrations of water in the reactor; however, FTS-GP appears to exhibit a higher tolerance for the added water than C_2H_4. On the other hand, as shown in Figure 8b, growth performed with FTS-GP exhibited a substantial

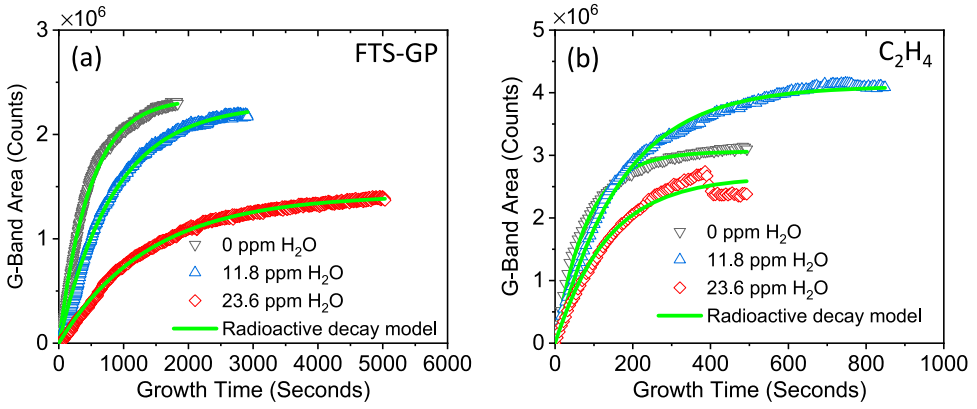

Figure 7. Plots of CNT yield as a function of growth time during CVD growth for different levels of water in ARES using FTS-GP (a) and ethylene (b) as feedstocks. The green solid lines represent curve fitting of the radioactive decay model (eq 1) to the experimental data shown in symbols.

https://dx.doi.org/10.1021/acs.iecr.0c00711
Ind. Eng. Chem. Res. 2020, 59, 9095−9104

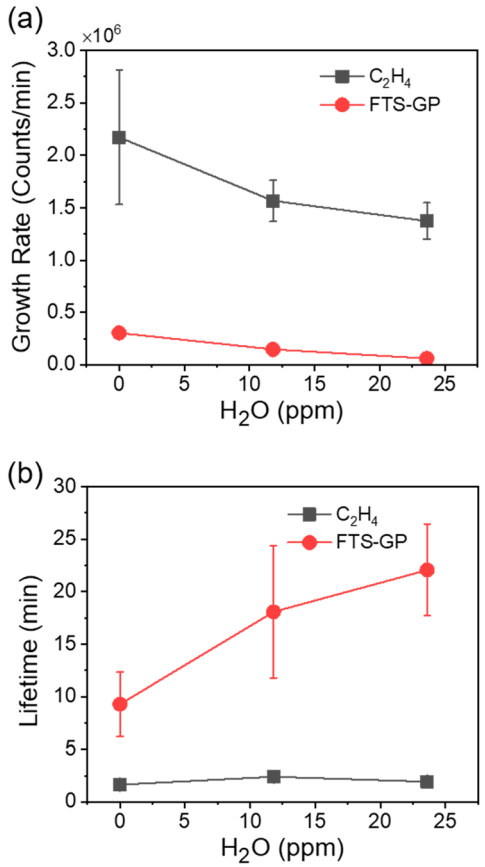

Figure 8. Growth kinetics parameters obtained by fitting the ARES growth curves with the radioactive decay model (eq 1). (a) Plots of initial growth rate of SWCNTs as a function of water concentrations for FTS-GP and ethylene. (b) Plots of catalyst lifetime as a function of water concentrations for FTS-GP and ethylene.

increase in lifetime with the addition of water, whereas growth with C_2H_4 exhibited a constant or even shortened catalyst lifetime with increasing concentrations of water. The remarkably long catalyst lifetimes observed for growth with FTS-GP compared to a standard feedstock indicates the high tolerance it has for relatively high levels of water near the catalysts, demonstrating a lifetime in the presence of 23.6 ppm water that is 11 times longer than that of C_2H_4.

Disparity in growth rates for experiments performed with FTS-GP and C_2H_4 may be due to factors such as a possible water gas shift reaction and poor utilization of methane in ARES. During SWCNT growth in a hot-wall CVD reactor, decomposition of the feedstock occurs in the gas phase and on the catalyst surface. On the other hand, ARES relies on heating from the laser, suggesting that gas phase reactions are extremely low or nonexistent; this feature is expected to not only limit the carbon flux to the catalyst but also the in situ water generation via reaction R1. In spite of these differences, SWCNTs produced by ARES using C_2H_4 and FTS-GP were of similar diameters compared to those grown in conventional CVD. Postgrowth Raman analysis of the SWCNTs revealed multiple RBMs between 100 and 300 cm^{-1} (Figure S2), similar to RBMs observed in conventional CVD growth experiments (Figure 3). High growth efficiency observed with FTS-GP in conventional CVD has been associated with the ability of the unsaturated hydrocarbon to dissociate in the gas phase, generating free radicals that attack the more stable hydrocarbons such as CH_4.[25] The process enhances the flux of carbon species to the surface while simultaneously inhibiting the catalyst deactivation pathways via reaction R1. Unfortunately, due to the absence of (or limited) gas-phase reactions in ARES, dissociation of CH_4 (40 vol % of FTS-GP) hardly occurs. This hypothesis is supported by the similarity in growth behavior between FTS-GP and the C_2H_4 and hydrogen mixture with no additional water (Figure S3). Significantly higher lifetimes measured with FTS-GP in comparison with C_2H_4 highlight the high tolerance of water with FTS.

The optimum concentration of water for "supergrowth" is still debatable, with most studies reporting values anywhere from 20 to 900 ppm.[8,10,12,57,58] However, a water concentration as low as 12 ppm has been reported by In et al.[59] to extend catalyst lifetime; in fact, the study concludes even a very small amount of water (~1 ppm) in a feed of high purity can dramatically affect the kinetics of SWCNT growth. Therefore, it is reasonable to assume the estimated water amounts produced by FTS-GP at 750 °C (64.6 ppm) in the vicinity of the catalyst are enough to protect the catalyst from deactivation. We speculate the optimum concentration of water in "supergrowth" is starkly different for different studies because of a variety of factors, including the type of feedstock, feed composition, and reactor geometry. As an example, Yasuda et al.[10] showed the optimum concentration of water during "supergrowth" changes with gas-flow direction, with top-flow growth showing relatively the highest sensitivity to water as opposed to lateral-flow growth. In addition, growth data from ARES reveal the poor water tolerance of C_2H_4, in agreement with the work of Xie et al.[23] that revealed a narrow range of water concentrations that support efficient growth. We hypothesize that water generated during FTS-GP CVD as depicted in Figure 1 will experience significantly fewer diffusion limitations and water level can be better controlled in comparison to water introduced with the feed as in "supergrowth"—making FTS-GP CVD more adaptable for scalable and controlled SWCNT growth.

Considering the complex composition of the feedstock and impact of gas-phase chemistry on CNT growth, the observed in situ generation of water may not be the only mechanism at play in the growth enhancement in FTS-GP CVD. Studies have revealed the formation of a broad population of specific hydrocarbon intermediates (volatile organic compounds and polycyclic aromatic compounds) in the gas phase for a conventional feedstock (C_2H_4), suggesting the existence of competing reaction pathways that may inhibit or enhance CNT carpet growth.[42,60,61] Under SWCNT growth conditions, it is also possible that the small Fe nanoparticles with high free energies may become highly reactive even for reactions that are not favorable under equilibrium conditions. However, in light of the critical role water plays in extending the catalyst lifetime during SWCNT growth as demonstrated by "supergrowth", we believe this study provides an important foundation for mechanistic development of this new process and will complement future mechanistic studies on cracking patterns of the hydrocarbons and interactions of the different species.

4. CONCLUSIONS

In this study, the role of FTS-GP in growth enhancement of FTS-GP CVD was studied using a combination of experimental and theoretical approaches. The results reveal in situ formation of water during FTS-GP CVD via a reaction between H_2 and the low-volume fraction of CO. The water

https://dx.doi.org/10.1021/acs.iecr.0c00711
Ind. Eng. Chem. Res. 2020, 59, 9095−9104

formed is expected to play a similar role as reported for "supergrowth". Catalytic performance (activity and lifetime) and the concentration of water formed during FTS-GP CVD experiments (or equilibrium partial pressure of water determined from thermodynamic calculations) are sensitive to the decomposition temperature of FTS-GP. Maximum carpet heights are achieved for growth at 650, 700, and 800 °C, and they are significantly lower than the experimental carpet height of ∼4 mm for growth at 750 °C that is still active after 90 min and experiences no sign of deactivation. Experiments conducted in ARES, in the presence of different amounts of water, revealed a higher overall yield of SWCNTs with C_2H_4 as the feedstock compared to FTS-GP. On the other hand, the catalyst lifetime for growth performed with FTS-GP exhibited a substantial increase with the addition of water, while growth with C_2H_4 exhibited a constant or even shortened catalyst lifetime with increasing concentrations of water. The ARES data support our mechanistic rationale for the observed growth enhancement with FTS-GP CVD. FTS-GP CVD has the combined advantage of supporting on-site generation of water and having a high tolerance for high concentrations of water, making process optimization and scale-up promising.

■ ASSOCIATED CONTENT

Supporting Information

The Supporting Information is available free of charge at https://pubs.acs.org/doi/10.1021/acs.iecr.0c00711.

Summary of predicted amount of water generated at different temperatures, plot of CNT yield (G-band intensity) versus growth temperature in ARES, post-growth Raman spectra collected from ARES micropillars (excitation wavelength 633 nm), and histograms of SWCNT yield (G-band intensity) and catalyst lifetime for different feedstocks and compositions in the absence of water (PDF)

■ AUTHOR INFORMATION

Corresponding Author

Placidus B. Amama − *Tim Taylor Department of Chemical Engineering, Kansas State University, Manhattan, Kansas 66506, United States;* orcid.org/0000-0001-9753-6044; Phone: 785-532-4318; Email: pamama@ksu.edu

Authors

Brian M. Everhart − *Tim Taylor Department of Chemical Engineering, Kansas State University, Manhattan, Kansas 66506, United States*

Haider Almkhelfe − *Tim Taylor Department of Chemical Engineering, Kansas State University, Manhattan, Kansas 66506, United States*

Xu Li − *Tim Taylor Department of Chemical Engineering, Kansas State University, Manhattan, Kansas 66506, United States*

Michael Wales − *Tim Taylor Department of Chemical Engineering, Kansas State University, Manhattan, Kansas 66506, United States*

Pavel Nikolaev − *Materials and Manufacturing Directorate, Air Force Research Laboratory, Wright-Patterson AFB, Ohio 45433, United States; UES Inc., Dayton, Ohio 45432, United States*

Rahul Rao − *Materials and Manufacturing Directorate, Air Force Research Laboratory, Wright-Patterson AFB, Ohio 45433, United States;* orcid.org/0000-0002-6415-0185

Benji Maruyama − *Materials and Manufacturing Directorate, Air Force Research Laboratory, Wright-Patterson AFB, Ohio 45433, United States*

Complete contact information is available at: https://pubs.acs.org/10.1021/acs.iecr.0c00711

Author Contributions

‖B.M.E. and H.A.: Equal contribution.

Notes

The authors declare no competing financial interest.

■ ACKNOWLEDGMENTS

This research was financially supported by the National Science Foundation (Award Nos. 1653527 and 1728567).

■ REFERENCES

(1) Almkhelfe, H.; Li, X.; Thapa, P.; Hohn, K. L.; Amama, P. B. Carbon Nanotube-Supported Catalysts Prepared by a Modified Photo-Fenton Process for Fischer−Tropsch Synthesis. *J. Catal.* **2018**, *361*, 278−289.

(2) Serp, P.; Machado, B. *Nanostructured Carbon Materials for Catalysis*; Royal Society of Chemistry: Cambridge, U.K., 2015.

(3) De las Casas, C.; Li, W. A Review of Application of Carbon Nanotubes for Lithium Ion Battery Anode Material. *J. Power Sources* **2012**, *208*, 74−85.

(4) Carter, R.; Oakes, L.; Cohn, A. P.; Holzgrafe, J.; Zarick, H. F.; Chatterjee, S.; Bardhan, R.; Pint, C. L. Solution Assembled Single-Walled Carbon Nanotube Foams: Superior Performance in Supercapacitors, Lithium-Ion, and Lithium−Air Batteries. *J. Phys. Chem. C* **2014**, *118*, 20137−20151.

(5) Cola, B. A.; Xu, X.; Fisher, T. S.; Capano, M. A.; Amama, P. B. Carbon Nanotube Array Thermal Interfaces for High-Temperature Silicon Carbide Devices. *Nanoscale Microscale Thermophys. Eng.* **2008**, *12*, 228−237.

(6) Cola, B. A.; Xu, X.; Fisher, T. S. Increased Real Contact in Thermal Interfaces: A Carbon Nanotube/Foil Material. *Appl. Phys. Lett.* **2007**, *90*, 093513.

(7) De Volder, M. F. L.; Tawfick, S. H.; Baughman, R. H.; Hart, A. J. Carbon Nanotubes: Present and Future Commercial Applications. *Science* **2013**, *339*, 535−539.

(8) Hata, K.; Futaba, D. N.; Mizuno, K.; Namai, T.; Yumura, M.; Iijima, S. Water-Assisted Highly Efficient Synthesis of Impurity-Free Single-Walled Carbon Nanotubes. *Science* **2004**, *306*, 1362−1364.

(9) Cohn, A. P.; Oakes, L.; Carter, R.; Chatterjee, S.; Westover, A. S.; Share, K.; Pint, C. L. Assessing the Improved Performance of Freestanding, Flexible Graphene and Carbon Nanotube Hybrid Foams for Lithium Ion Battery Anodes. *Nanoscale* **2014**, *6*, 4669−4675.

(10) Yasuda, S.; Futaba, D. N.; Yamada, T.; Satou, J.; Shibuya, A.; Takai, H.; Arakawa, K.; Yumura, M.; Hata, K. Improved and Large Area Single-Walled Carbon Nanotube Forest Growth by Controlling the Gas Flow Direction. *ACS Nano* **2009**, *3*, 4164−4170.

(11) Lee, J.; Oh, E.; Kim, T.; Sa, J.-H.; Lee, S.-H.; Park, J.; Moon, D.; Kang, I. S.; Kim, M. J.; Kim, S. M.; Lee, K.-H. The Influence of Boundary Layer on the Growth Kinetics of Carbon Nanotube Forests. *Carbon* **2015**, *93*, 217−225.

(12) Rao, R.; Pint, C. L.; Islam, A. E.; Weatherup, R. S.; Hofmann, S.; Meshot, E. R.; Wu, F.; Zhou, C.; Dee, N.; Amama, P. B.; Carpena-Nuñez, J.; Shi, W.; Plata, D. L.; Penev, E. S.; Yakobson, B. I.; Balbuena, P. B.; Bichara, C.; Futaba, D. N.; Noda, S.; Shin, H.; Kim, K. S.; Simard, B.; Mirri, F.; Pasquali, M.; Fornasiero, F.; Kauppinen, E. I.; Arnold, M.; Cola, B. A.; Nikolaev, P.; Arepalli, S.; Cheng, H.-M.; Zakharov, D. N.; Stach, E. A.; Zhang, J.; Wei, F.; Terrones, M.; Geohegan, D. B.; Maruyama, B.; Maruyama, S.; Li, Y.; Adams, W. W.; Hart, A. J. Carbon Nanotubes and Related Nanomaterials: Critical

Advances and Challenges for Synthesis toward Mainstream Commercial Applications. *ACS Nano* **2018**, *12*, 11756−11784.
(13) Futaba, D. N.; Hata, K.; Yamada, T.; Mizuno, K.; Yumura, M.; Iijima, S. Kinetics of Water-Assisted Single-Walled Carbon Nanotube Synthesis Revealed by a Time-Evolution Analysis. *Phys. Rev. Lett.* **2005**, *95*, 056104.
(14) Meshot, E. R.; Park, S. J.; Buchsbaum, S. F.; Jue, M. L.; Kuykendall, T. R.; Schaible, E.; Bayu Aji, L. B.; Kucheyev, S. O.; Wu, K. J. J.; Fornasiero, F. High-Yield Growth Kinetics and Spatial Mapping of Single-Walled Carbon Nanotube Forests at Wafer Scale. *Carbon* **2020**, *159*, 236−246.
(15) Zhang, Y.; Gregoire, J. M.; van Dover, R. B.; Hart, A. J. Ethanol-Promoted High-Yield Growth of Few-Walled Carbon Nanotubes. *J. Phys. Chem. C* **2010**, *114*, 6389−6395.
(16) Sugime, H.; Noda, S. Millimeter-Tall Single-Walled Carbon Nanotube Forests Grown from Ethanol. *Carbon* **2010**, *48*, 2203−2211.
(17) Dai, H.; Rinzler, A. G.; Nikolaev, P.; Thess, A.; Colbert, D. T.; Smalley, R. E. Single-Wall Nanotubes Produced by Metal-Catalyzed Disproportionation of Carbon Monoxide. *Chem. Phys. Lett.* **1996**, *260*, 471−475.
(18) Zheng, B.; Lu, C.; Gu, G.; Makarovski, A.; Finkelstein, G.; Liu, J. Efficient CVD Growth of Single-Walled Carbon Nanotubes on Surfaces Using Carbon Monoxide Precursor. *Nano Lett.* **2002**, *2*, 895−898.
(19) Futaba, D. N.; Goto, J.; Yasuda, S.; Yamada, T.; Yumura, M.; Hata, K. General Rules Governing the Highly Efficient Growth of Carbon Nanotubes. *Adv. Mater.* **2009**, *21*, 4811−4815.
(20) Magrez, A.; Seo, J. W.; Kuznetsov, V. L.; Forró, L. Evidence of an Equimolar C_2H_2−CO_2 Reaction in the Synthesis of Carbon Nanotubes. *Angew. Chem., Int. Ed.* **2007**, *46*, 441−444.
(21) Wen, Q.; Qian, W.; Wei, F.; Liu, Y.; Ning, G.; Zhang, Q. CO_2-Assisted Swnt Growth on Porous Catalysts. *Chem. Mater.* **2007**, *19*, 1226−1230.
(22) Sato, T.; Sugime, H.; Noda, S. CO_2-Assisted Growth of Millimeter-Tall Single-Wall Carbon Nanotube Arrays and Its Advantage against H_2O for Large-Scale and Uniform Synthesis. *Carbon* **2018**, *136*, 143−149.
(23) Xie, K.; Muhler, M.; Xia, W. Influence of Water on the Initial Growth Rate of Carbon Nanotubes from Ethylene over a Cobalt-Based Catalyst. *Ind. Eng. Chem. Res.* **2013**, *52*, 14081−14088.
(24) Szabó, A.; Kecsenovity, E.; Pápa, Z.; Gyulavári, T.; Németh, K.; Horvath, E.; Hernadi, K. Influence of Synthesis Parameters on CCVD Growth of Vertically Aligned Carbon Nanotubes over Aluminum Substrate. *Sci. Rep.* **2017**, *7*, 9557.
(25) Almkhelfe, H.; Carpena-Nunez, J.; Back, T. C.; Amama, P. B. Gaseous Product Mixture from Fischer−Tropsch Synthesis as an Efficient Carbon Feedstock for Low Temperature CVD Growth of Carbon Nanotube Carpets. *Nanoscale* **2016**, *8*, 13476−13487.
(26) Almkhelfe, H.; Li, X.; Rao, R.; Amama, P. B. Catalytic CVD Growth of Millimeter-Tall Single-Wall Carbon Nanotube Carpets Using Industrial Gaseous Waste as a Feedstock. *Carbon* **2017**, *116*, 181−190.
(27) Jahangiri, H.; Bennett, J.; Mahjoubi, P.; Wilson, K.; Gu, S. A Review of Advanced Catalyst Development for Fischer−Tropsch Synthesis of Hydrocarbons from Biomass Derived Syn-Gas. *Catal. Sci. Technol.* **2014**, *4*, 2210−2229.
(28) Almkhelfe, H. Scalable Carbon Nanotube Growth and Design of Efficient Catalysts for Fischer−Tropsch Synthesis. Ph.D. Dissertation, Kansas State University, 2017.
(29) Yamada, T.; Maigne, A.; Yudasaka, M.; Mizuno, K.; Futaba, D. N.; Yumura, M.; Iijima, S.; Hata, K. Revealing the Secret of Water-Assisted Carbon Nanotube Synthesis by Microscopic Observation of the Interaction of Water on the Catalysts. *Nano Lett.* **2008**, *8*, 4288−4292.
(30) Amama, P. B.; Pint, C. L.; McJilton, L.; Kim, S. M.; Stach, E. A.; Murray, P. T.; Hauge, R. H.; Maruyama, B. Role of Water in Super Growth of Single-Walled Carbon Nanotube Carpets. *Nano Lett.* **2009**, *9*, 44−49.
(31) Kim, S.; Pint, C.; Amama, P.; Zakharov, D.; Hauge, R.; Maruyama, B.; Stach, E. Understanding Growth Termination of Single-Walled Carbon Nanotube Carpets by Documenting the Evolution of Catalyst Morphology with the Transmission Electron Microscope. *Microsc. Microanal.* **2009**, *15*, 1176.
(32) Kim, S. M.; Pint, C. L.; Amama, P. B.; Hauge, R. H.; Maruyama, B.; Stach, E. A. Catalyst and Catalyst Support Morphology Evolution in Single-Walled Carbon Nanotube Supergrowth: Growth Deceleration and Termination. *J. Mater. Res.* **2010**, *25*, 1875−1885.
(33) Kim, S. M.; Pint, C. L.; Amama, P. B.; Zakharov, D. N.; Hauge, R. H.; Maruyama, B.; Stach, E. A. Evolution in Catalyst Morphology Leads to Carbon Nanotube Growth Termination. *J. Phys. Chem. Lett.* **2010**, *1*, 918−922.
(34) Amama, P. B.; Pint, C. L.; Kim, S. M.; McJilton, L.; Eyink, K. G.; Stach, E. A.; Hauge, R. H.; Maruyama, B. Influence of Alumina Type on the Evolution and Activity of Alumina-Supported Fe Catalysts in Single-Walled Carbon Nanotube Carpet Growth. *ACS Nano* **2010**, *4*, 895−904.
(35) Amama, P. B.; Pint, C. L.; Mirri, F.; Pasquali, M.; Hauge, R. H.; Maruyama, B. Catalyst−Support Interactions and Their Influence in Water-Assisted Carbon Nanotube Carpet Growth. *Carbon* **2012**, *50*, 2396−2406.
(36) Nikolaev, P.; Hooper, D.; Webber, F.; Rao, R.; Decker, K.; Krein, M.; Poleski, J.; Barto, R.; Maruyama, B. Autonomy in Materials Research: A Case Study in Carbon Nanotube Growth. *npj Comput. Mater.* **2016**, *2*, 16031.
(37) Nikolaev, P.; Hooper, D.; Perea-Lopez, N.; Terrones, M.; Maruyama, B. Discovery of Wall-Selective Carbon Nanotube Growth Conditions Via Automated Experimentation. *ACS Nano* **2014**, *8*, 10214−10222.
(38) Hall, W. K.; Kokes, R. J.; Emmett, P. H. Mechanism Studies of the Fischer−Tropsch Synthesis. The Addition of Radioactive Methanol, Carbon Dioxide and Gaseous Formaldehyde. *J. Am. Chem. Soc.* **1957**, *79*, 2983−2989.
(39) Kibby, C.; Jothimurugesan, K.; Das, T.; Lacheen, H. S.; Rea, T.; Saxton, R. J. Chevron's Gas Conversion Catalysis-Hybrid Catalysts for Wax-Free Fischer−Tropsch Synthesis. *Catal. Today* **2013**, *215*, 131−141.
(40) Tavasoli, A.; Sadagiani, K.; Khorashe, F.; Seifkordi, A. A.; Rohani, A. A.; Nakhaeipour, A. Cobalt Supported on Carbon Nanotubes — a Promising Novel Fischer−Tropsch Synthesis Catalyst. *Fuel Process. Technol.* **2008**, *89*, 491−498.
(41) Zgolicz, P. D.; Stassi, J. P.; Yañez, M. J.; Scelza, O. A.; de Miguel, S. R. Influence of the Support and the Preparation Methods on the Performance in Citral Hydrogenation of Pt-Based Catalysts Supported on Carbon Nanotubes. *J. Catal.* **2012**, *290*, 37−54.
(42) Meshot, E. R.; Plata, D. L.; Tawfick, S.; Zhang, Y.; Verploegen, E. A.; Hart, A. J. Engineering Vertically Aligned Carbon Nanotube Growth by Decoupled Thermal Treatment of Precursor and Catalyst. *ACS Nano* **2009**, *3*, 2477−2486.
(43) Einarsson, E.; Murakami, Y.; Kadowaki, M.; Maruyama, S. Growth Dynamics of Vertically Aligned Single-Walled Carbon Nanotubes from in Situ Measurements. *Carbon* **2008**, *46*, 923−930.
(44) Li, X.; Gray, E. R.; Islam, A. E.; Sargent, G. A.; Maruyama, B.; Amama, P. B. Magnesia and Magnesium Aluminate Catalyst Substrates for Carbon Nanotube Carpet Growth. *ACS Applied Nano Materials* **2020**, *3*, 1830−1840.
(45) Miura, S.; Yoshihara, Y.; Asaka, M.; Hasegawa, K.; Sugime, H.; Ota, A.; Oshima, H.; Noda, S. Millimeter-Tall Carbon Nanotube Arrays Grown on Aluminum Substrates. *Carbon* **2018**, *130*, 834−842.
(46) Eres, G.; Kinkhabwala, A. A.; Cui, H.; Geohegan, D. B.; Puretzky, A. A.; Lowndes, D. H. Molecular Beam-Controlled Nucleation and Growth of Vertically Aligned Single-Wall Carbon Nanotube Arrays. *J. Phys. Chem. B* **2005**, *109*, 16684−16694.
(47) Zhong; Iwasaki, T.; Robertson, J.; Kawarada, H. Growth Kinetics of 0.5 Cm Vertically Aligned Single-Walled Carbon Nanotubes. *J. Phys. Chem. B* **2007**, *111*, 1907−1910.
(48) Xu, Y.-Q.; Flor, E.; Kim, M. J.; Hamadani, B.; Schmidt, H.; Smalley, R. E.; Hauge, R. H. Vertical Array Growth of Small Diameter

https://dx.doi.org/10.1021/acs.iecr.0c00711
Ind. Eng. Chem. Res. 2020, 59, 9095−9104

Single-Walled Carbon Nanotubes. *J. Am. Chem. Soc.* **2006**, *128*, 6560−6561.
(49) Xiang, R.; Einarsson, E.; Okawa, J.; Miyauchi, Y.; Maruyama, S. Acetylene-Accelerated Alcohol Catalytic Chemical Vapor Deposition Growth of Vertically Aligned Single-Walled Carbon Nanotubes. *J. Phys. Chem. C* **2009**, *113*, 7511−7515.
(50) Noda, S.; Hasegawa, K.; Sugime, H.; Kakehi, K.; Zhang, Z.; Maruyama, S.; Yamaguchi, Y. Millimeter-Thick Single-Walled Carbon Nanotube Forests: Hidden Role of Catalyst Support. *Jpn. J. Appl. Phys.* **2007**, *46*, L399.
(51) Hasegawa, K.; Noda, S. Real-Time Monitoring of Millimeter-Tall Vertically Aligned Single-Walled Carbon Nanotube Growth on Combinatorial Catalyst Library. *Jpn. J. Appl. Phys.* **2010**, *49*, 085104.
(52) Yasuda, S.; Futaba, D. N.; Yamada, T.; Yumura, M.; Hata, K. Gas Dwell Time Control for Rapid and Long Lifetime Growth of Single-Walled Carbon Nanotube Forests. *Nano Lett.* **2011**, *11*, 3617−3623.
(53) Chen, G.; Davis, R. C.; Kimura, H.; Sakurai, S.; Yumura, M.; Futaba, D. N.; Hata, K. The Relationship between the Growth Rate and the Lifetime in Carbon Nanotube Synthesis. *Nanoscale* **2015**, *7*, 8873−8878.
(54) Moisala, A.; Nasibulin, A. G.; Kauppinen, E. I. The Role of Metal Nanoparticles in the Catalytic Production of Single-Walled Carbon Nanotubes—a Review. *J. Phys.: Condens. Matter* **2003**, *15*, S3011.
(55) Nasibulin, A. G.; Moisala, A.; Brown, D. P.; Kauppinen, E. I. Carbon Nanotubes and Onions from Carbon Monoxide Using Ni(Acac)2 and Cu(Acac)2 as Catalyst Precursors. *Carbon* **2003**, *41*, 2711−2724.
(56) Bale, C. W.; Chartrand, P.; Decterov, S. A.; Eriksson, G.; Hack, K.; Jung, I. H.; Kang, Y. B.; Melançon, J.; Pelton, A. D.; Robelin, C.; Petersen, S.; Bélisle, E. FactSage thermochemical software and databases − recent developments. *CALPHAD: Comput. Coupling Phase Diagrams Thermochem.* **2009**, *33*, 295−311.
(57) Yamada, T.; Namai, T.; Hata, K.; Futaba, D. N.; Mizuno, K.; Fan, J.; Yudasaka, M.; Yumura, M.; Iijima, S. Size-Selective Growth of Double-Walled Carbon Nanotube Forests from Engineered Iron Catalysts. *Nat. Nanotechnol.* **2006**, *1*, 131−136.
(58) Cho, W.; Schulz, M.; Shanov, V. Kinetics of Growing Centimeter Long Carbon Nanotube Arrays. In *Syntheses and Applications of Carbon Nanotubes and Their Composites*; InTech: 2013. DOI: 10.5772/50837.
(59) In, J. B.; Grigoropoulos, C. P.; Chernov, A. A.; Noy, A. Hidden Role of Trace Gas Impurities in Chemical Vapor Deposition Growth of Vertically-Aligned Carbon Nanotube Arrays. *Appl. Phys. Lett.* **2011**, *98*, 153102.
(60) Plata, D. L.; Meshot, E. R.; Reddy, C. M.; Hart, A. J.; Gschwend, P. M. Multiple Alkynes React with Ethylene to Enhance Carbon Nanotube Synthesis, Suggesting a Polymerization-Like Formation Mechanism. *ACS Nano* **2010**, *4*, 7185−7192.
(61) Nessim, G. D.; Seita, M.; Plata, D. L.; O'Brien, K. P.; John Hart, A.; Meshot, E. R.; Reddy, C. M.; Gschwend, P. M.; Thompson, C. V. Precursor Gas Chemistry Determines the Crystallinity of Carbon Nanotubes Synthesized at Low Temperature. *Carbon* **2011**, *49*, 804−810.

https://dx.doi.org/10.1021/acs.iecr.0c00711
Ind. Eng. Chem. Res. 2020, 59, 9095−9104